PASJ: Publ. Astron. Soc. Japan **46**, L59–L63 (1994)

ASCA Observations of the Warm Absorber in MCG−6–30–15: the Discovery of a Change in Column Density

Andrew C. FABIAN,[1,2] Hideyo KUNIEDA,[3] Shigeru INOUE,[3]
Masaru MATSUOKA,[4] Tatehiro MIHARA,[4] Sigenori MIYAMOTO,[5] Chiko OTANI,[1]
George RICKER,[6] Yasuo TANAKA,[1] Makoto YAMAUCHI,[4] and Tahir YAQOOB[7]

[1]*Institute of Space and Astronautical Science, 3-1-1 Yoshinodai, Sagamihara, Kanagawa 229*
[2]*Institute of Astronomy, Madingley Road, Cambridge CB3 0HA, UK*
[3]*Department of Astrophysics, Nagoya University, Furo-cho, Chikusa, Nagoya 464*
[4]*Institute of Physical and Chemical Research (RIKEN), Hirosawa, Wako, Saitama 351-01*
[5]*Department of Earth and Space Science, Osaka University, Machikaneyama , Toyonaka, Osaka 560*
[6]*Department of Space Research, Massachusetts Institute of Technology, Cambridge MA 02139, USA*
[7]*Laboratory for High Energy Astrophysics, NASA/GSFC, Greenbelt, MD20771, USA*

(Received 1994 January 28; accepted 1994 March 29)

Abstract

We report the first X-ray observations of the Seyfert 1 galaxy MCG−6–30–15 obtained at medium spectral resolution. The partially-ionized, 'warm' absorber is resolved and shown to be due to O VII and O VIII. The main absorption edge agrees with that of O VII at the redshift of the galaxy to within 1%. The column density of the absorbing material is greater by a factor of 2 in the first of our two observations, which were 3 weeks apart, whilst the mean flux is slightly lower and the ionization parameter slightly higher. We also discuss the fluorescent iron emission line seen in the source, which is at 6.40 keV. The line is significantly broadened, with a FWHM of about 0.4 keV.

Key words: Galaxies: individual (MCG−6–30–15) — Galaxies: Seyfert — Line: profiles — X-rays: galaxies

1. Introduction

The bright Seyfert 1 galaxy MCG−6–30–15 has been well studied in X-rays (Pounds et al. 1986, 1990; Matsuoka et al. 1990; Nandra et al. 1990; Fiore et al. 1992). It shows rapid X-ray variability on timescales down to below 1000 s, and a complex X-ray spectrum. The spectral features above a few keV are well-explained by a model in which a power-law continuum irradiates a surrounding cold matter to produce a reflection component consisting of a hard continuum and fluorescent iron line (see Guilbert, Rees 1988; Lightman, White 1988; George, Fabian 1991; Matt et al. 1991). Excess emission has been reported at soft energies and, most recently, a large absorption feature due to oxygen (Nandra, Pounds 1992). The absorption is at an energy consistent with the K-edges of O VII and O VIII which indicates that it occurs in warm, partially-ionized, matter along the line of sight. Warm absorbers have also been found in other Seyfert galaxies (Halpern 1984; Yaqoob et al. 1989; Pan et al. 1990; Nandra, Pounds 1992; Turner et al. 1993) and are discussed from a theoretical point of view by Netzer (1993).

The effect of warm absorption is detectable in the emergent spectrum above 2 keV and further complicates our understanding of the nature of the underlying continuum, such as its spectral index and whether it is a true power-law over several decades of photon energy. We now recognize that reprocessing affects much of the X-ray spectrum of Seyfert galaxies. The energy band over which the raw continuum dominates the observed spectrum is limited to perhaps the 3–5 keV band only, if we allow for the possibility that the iron line is broad. In order to understand the spectrum in detail requires that all features be modelled well, which in turn requires good spectral resolution.

Here we report the first observations of MCG−6–30–15 with the fourth Japanese X-ray astronomy satellite named ASCA, which has imaging CCDs and GSPCs with energy-dependent resolutions of 50–150 eV and 300–600 eV, respectively. The warm absorption edges and iron emission line are clearly resolved for the first time. We have also discovered a large change in the column density of the warm absorber between the first observation in 1993 July and the second one in August.

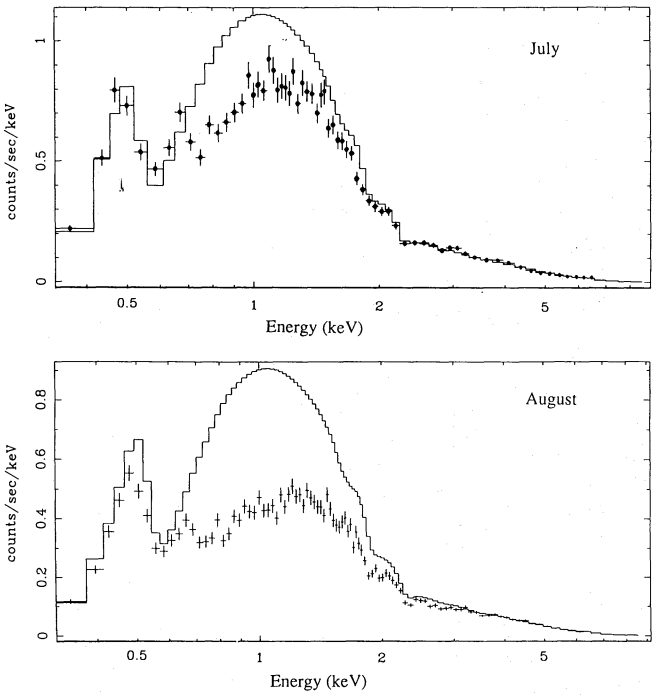

Fig. 1. SIS 1 spectra of MCG−6−30−15 taken in July (top panel) and August (lower panel). The model spectrum shown is the power-law spectrum (with Galactic absorption) that best fits both data jointly in above 3.2 keV. Note the large deficit of counts between 0.7 and ∼ 2 keV.

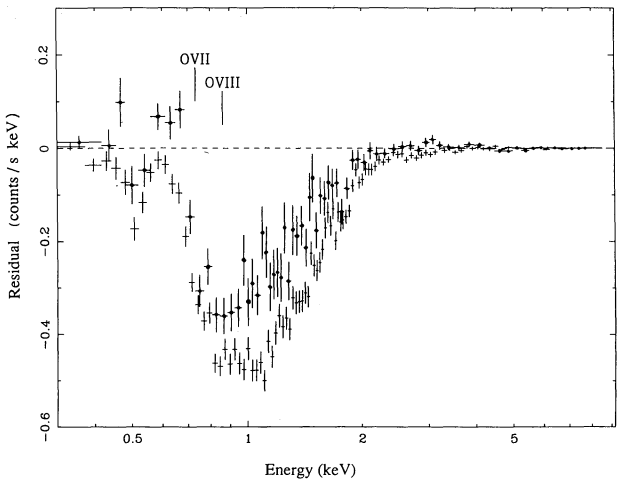

Fig. 2. Comparison of the residuals from the spectra shown in figure 1. Note that the drop in counts sets in at the O VII edge. There may also be possible features at lower energy (C VI and N VI) and at higher energy (O VIII and Ne IX).

2. The X-Ray Data

MCG−6−30−15 was observed by ASCA on 1993 July 8–9 and July 31–August 1 (hereafter, the July and August datasets). In this paper we centre the discussion on data from one of the two CCD Solid-State Imaging Spectrometers. Data were also collected with SIS 0 and the two Gas Imaging Spectrometers. The SIS were operated in 2-CCD mode with the source centred on one of the detectors. We further restrict the data discussed here to that collected in bright mode.

Hot pixels were removed from the SIS data and periods of high count rate due to background are rejected. Spectra were then accumulated from a circular region of radius 3′.1 about the centre of the image of the source. Channels from at most 0.35 to 9 keV have then been fitted with model spectra using XSPEC and response matrices appropriate for an off-axis source. The source showed significant variability on timescales down to about 1000 s in both datasets.

The spectra obtained from the July (11264 s) and August (30766 s) data are shown separately in figure 1. A power-law spectrum with Galactic absorption (corresponding to a hydrogen column density of 5×10^{20} cm^{-2}) has been fitted to the data above 3.2 keV then extrapolated to the softer energy band. A gaussian emission line has been included around the iron K energy (6.4 keV) and maximum likelihood statistics used since the number of counts per channel is small at the higher energies. The parameters of the best-fitting spectrum are photon index $\Gamma \approx 2$, line energy = 6.350 keV and the equivalent width of the line is ∼ 160 eV in July and ∼ 200 eV in August. The quality of the fit above 3 keV appears good, with no large features in the residuals (data–model). No background subtraction has been carried out due to the preliminary state of the software, but we can expect that any such subtraction would cause the required power-law to steepen. Comparison with the background (internal and cosmic) measured in deep fields shows that it only becomes comparable to the flux measured for MCG−6−30−15 above 9 keV. The GIS spectra are also consistent with a steep power-law model, $\Gamma \approx 1.85$ above 3 keV.

3. Interpretation

It is immediately apparent that there is a large difference between the extrapolated spectrum and the data, for both data sets in SIS and also in GIS data. The dominant effect is of an absorption feature, that sets in at about 0.73 keV, consistent with the O VII edge (figure 2). The difference in the feature between the datasets is more in depth than shape, indicating that the effect is more of an increase in the optical depth of the absorber than a change in its ionization state.

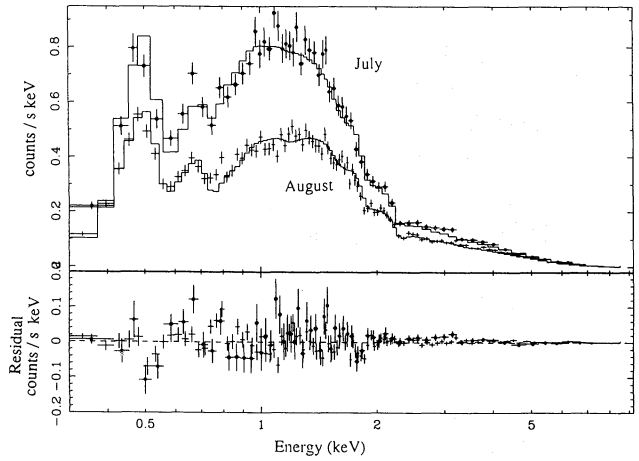

Fig. 3. Best-fitting (maximum likelihood) warm absorber model with a blackbody included in the incident spectrum. Details of the parameters are given in the text. Among the major remaining residuals, at 0.5, 0.8, and 1.8 keV, note that there is some evidence for an O VIII edge in the residuals, indicating that the absorber is more complicated than the models attempted so far.

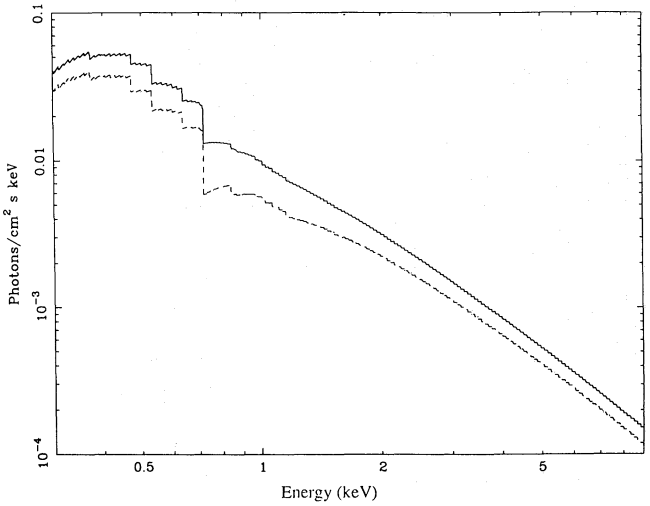

Fig. 4. Intrinsic spectra of the models shown in figure 3. The change in column density is clearly seen between the July (upper) and August (lower).

The spectra have been fitted with a simple model consisting of Galactic absorption, plus an edge acting on a power-law. When fit simultaneously to both the July and August spectra, with the only the edge depth and power-law normalization being allowed to differ, the photon index is found to be $\Gamma = 2.01^{+0.03}_{-0.01}$ and the edge begins at $0.739^{+0.01}_{-0.007}$ keV (all uncertainties are quoted at the 90% confidence level). This is consistent with O VII at the redshift of MCG−6−30−15 (0.008, which shifts the edge threshold to 0.733 keV). The optical depth of the edge is 0.57 ± 0.06 in July and $1.17^{+0.05}_{-0.01}$ in August (χ^2/d.o.f. = 1368/792). The results are little changed if the power-law index is allowed to be different for each spectrum. Also the August edge properties are consistent with those determined from fits to $\sim$ 1000 s long spectra obtained from the brightest and dimmest parts of the source light curve.

Although the result appears to be dominated by absorption by O VII, it is plausible that other ionization species of oxygen and other elements are also absorbing some of the X-rays. This is borne out by inspection of the fits and by fitting the different datasets separately. A grid of self-consistent models has therefore been produced using Ferland's (1991) photoionization code CLOUDY. This enables the spectrum emergent from a photoionized cloud to be computed for various cloud densities, ionizing fluxes, and geometries. Initially a power-law ionizing continuum has been used, of photon index $\Gamma = 2$ and luminosity 10^{43} erg s^{-1}, incident onto a shell at inner radius 10^{16} cm of density 10^8–10^{10} cm^{-1}. This means that the ionization parameter $\xi = L/nR^2$ varies from 10 to 1000. The column density varies from $N_{\rm W} = 10^{21.3}$–$10^{23.3}$ cm^{-2}. The shell is always thinner than the inner radius (usually very much thinner) so that the geometry is essentially plane-parallel. The emergent spectrum consists of both the transmitted continuum and the emission produced by the shell itself.

This model gives a significantly better fit ($\chi^2 = 1081$) and determines $\log N_{\rm W}$ and ξ to be 21.8 ± 0.1 and $39.0^{+7.5}_{-5.}$ in July and 22.13 ± 0.02 and 44.7 ± 3 in August. As deduced from the simple absorption edge fit, the difference in the spectra is mainly due to a factor of 2 change in the column density between the two observations. As the mean underlying continuum has decreased from July to August the column density has increased. The ionization parameter has also increased contrary to simple expectations if the absorbing matter were a constant density cloud responding to the ionizing continuum. The result is also robust to redshift changes of a few per cent, indicating that the absorbing matter is not in some high velocity bulk flow. Computing a new grid of models in which only the effects of absorption on the continuum and no emission features are included, has no significant effect on the overall fit. This means that at this stage we cannot distinguish between absorption in a small cloud along the line-of sight (little emission expected) or a complete shell surrounding the source (maximum emission expected if the shell is isotropic).

The models indicate that there is no simple explanation for the change in column density in terms of part of the cloud which was highly ionized in July when the flux

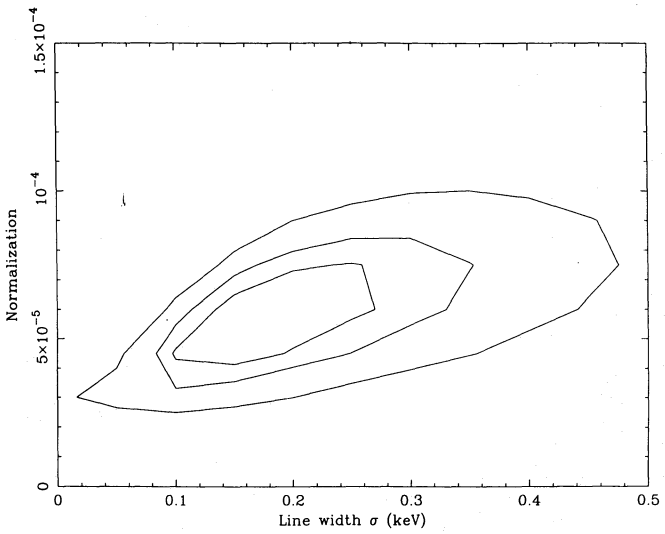

Fig. 5. Confidence contours for the line width and normalization of the gaussian iron-emission line fitted jointly to the 3.2–9 keV band of the August SIS 0 and 1 spectra. Contour levels correspond to 68, 90, and 99% confidence levels from outside to inside.

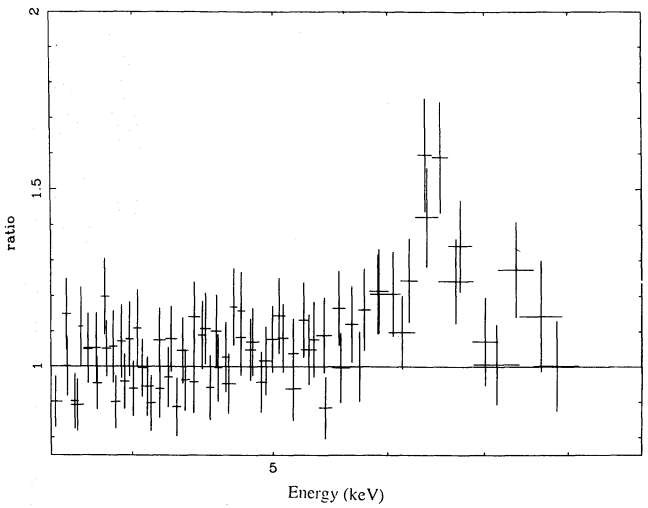

Fig. 6. Ratio of the data to the best-fitting model (with the line strength set to zero). Note the clear line feature around 6.4 keV.

was slightly higher (count rate 1.413 ± 0.011 ct s^{-1} against 0.913 ± 0.005 ct s^{-1} in August for the aperture chosen on the image). If we assume that the site of the underlying emission is unchanged then the absorbing matter must have changed.

Finally, we have investigated a model in which a soft excess contributes to the underlying spectrum by adding a blackbody spectrum. Although such a model gives a crude fit to the spectra without any warm absorption if a broad (oxygen) emission line is added (mimicking the drop which occurs at an O VII edge), we dismiss it since it leads to a broad hump in the residuals around 2–3 keV; the data above 0.8 keV cannot be fit by a simple power-law. Instead we include it in the incident spectrum for the CLOUDY grid, at a luminosity of about 10% of the power-law and with a temperature of 0.13 keV (chosen after trial fits with a blackbody added on top of the earlier models). This yields the best agreement so far ($\chi^2 = 1018$; figure 3) with $(\log N_{\rm W}, \xi) = (21.56, 11.09)$ in July and $(21.84, 14.6)$ in August. The blackbody requires a deeper edge which improves the fit around 1 keV (figure 4), which was unsatisfactory in the earlier models. Note that the factor of 2 change in column density is robust. The largest residuals in the fits now occur at about 0.5 and 1.8 keV where there are sharp features in the detector response matrix due to oxygen and silicon, and are unlikely to have a cosmic origin.

4. The Iron Line

The 6.4 keV iron emission line appears to be detected at a higher significance in the August data, where at this stage of the analysis we have a much longer integration time. Therefore for analysis of the iron line, spectra of the source from SIS 0 and 1 have been accumulated and fitted jointly with the simple absorbed power-law plus edge and gaussian line model. The energy band is then restricted to 3.2–9 keV. The parameters are very similar to those obtained with SIS 1 alone, the iron line being most significant in the SIS 0 detector. To obtain the details of the iron line the absorption parameters and the photon index have been fixed in subsequent spectral fitting ($\Gamma = 2$).

The line centroid is at $6.40^{+0.09}_{-0.05}$ keV and the line width (standard deviation of the gaussian) is $0.16^{+0.16}_{-0.06}$ keV and the equivalent width 210 eV. The allowed range of line normalization and width are shown in figure 5 and, after setting the line normalization to zero, the ratio of data/model as a function of energy is shown in figure 6. This last plot clearly shows the line feature.

Further ASCA work must await a more detailed analysis involving background subtraction and the GIS spectra (which are more sensitive at higher energies). We shall also include a more detailed model of the reflected continuum and in particular the iron edge in that component, which may account for some of the strength of the iron emission determined here. A preliminary check on this using the simple reflection model in XSPEC indicates that this is not a large effect.

An emission line of the shape expected from reflection

by the inner regions of a relativistic disk has also been fitted to the spectra. No improvement in χ^2 was found (349 for 330 spectral bins). The centroid line energy is 6.41 keV, the equivalent width 270 eV and the disk inclination about 25° (range $\sim$ 10°–45°).

5. Conclusion

We have confirmed the presence of a warm absorber in the Seyfert 1 galaxy MCG−6–30–15. The dominant edge energy is consistent to within 1 per cent of that expected from O VII. The column density of the absorber increased by about a factor of 2 between 1993 July and August.

The ASCA data show the iron emission line discovered from Ginga and reveal that it is broad, with a FWHM of about 400 eV, and has an equivalent width of about 200 eV. Further work with the complete dataset should refine and reveal more about this interesting source.

The authors wish to express their thanks to the launch team of the Institute of Space and Astronautical Science and all the ASCA team members whose effort made these observations and data analysis possible. ACF thanks ISAS for support and hospitality during the summer of 1993.

References

Ferland G.J. 1991, OSU Internal Report No. 91-01
Fiore F., Perola G.C., Matsuoka M., Yamauchi M., Piro L. 1992, A&A 262, 37
George I.M., Fabian A.C. 1991, MNRAS 249, 352
Guilbert P.W., Rees M.J. 1988, MNRAS 233, 475
Halpern J.P. 1984, ApJ 281, 90
Lightmann A.P., White T.R. 1988, ApJ 335, 57
Matsuoka M., Piro L., Yamauchi M., Murakami T. 1990, ApJ 361, 440
Matt G., Perola G.C., Piro L. 1991, A&A 247, 25
Nandra K., Pounds K.A., Stewart G.C. 1990, MNRAS 242, 660
Nandra K., Pounds K.A. 1992, Nature 359, 215
Nandra K., Fabian A.C., George I.M., Branduardi-Raymont G., Lawrence A., Mason K.O., McHardy I.M., Pounds K.A. et al. 1993, MNRAS 260, 504
Netzer H. 1993, ApJ 411, 594
Pan H.C., Stewart G.C., Pounds K.A. 1990, MNRAS 242, 177
Pounds K.A., Turner T.J., Warwick R.S. 1986, MNRAS 221, 7
Pounds K.A., Nandra K., Stewart G.C., George I.M., Fabian A.C. 1990, Nature 344, 132
Turner T.J., Nandra K., George I.M., Fabian A.C., Pounds K.A. 1993, ApJ 419, 127
Yaqoob T., Warwick R.S., Pounds K.A. 1989, MNRAS 236, 153